Supervised classification of remote sensing images including urban areas by using Markovian models

Aurélie Voisin, Vladimir Krylov, Josiane Zerubia

INRIA Sophia Antipolis Méditerranée (France), Ayin team,
in collaboration with the University of Genoa (Italy), DITEN department
Publications available on https://team.inria.fr/ayin/aurelie-voisin/

October 2012

Introduction

Objectives:

- Supervised image classifiers.
- General and sufficiently robust to different types of images.

Applications:

- Remote sensing, skin-care.
- Focus on (single-pol) radar (SAR) imagery, and extension to multi-resolution and/or multi-sensor data (SAR/optical).

SAR imagery

©ASI

- All-weather conditions.
- Polarimetric radar: SAR amplitude.
- SpotLight ($\sim$ 1m), StripMap ($\sim$ 2.5m), PingPong ($\sim$ 5m).
- Challenge: Speckle noise.

Optical imagery

©GeoEye

- Here considered as an additional information to SAR.

Example of SAR data classification

(a) SAR image (©ASI, 2008)

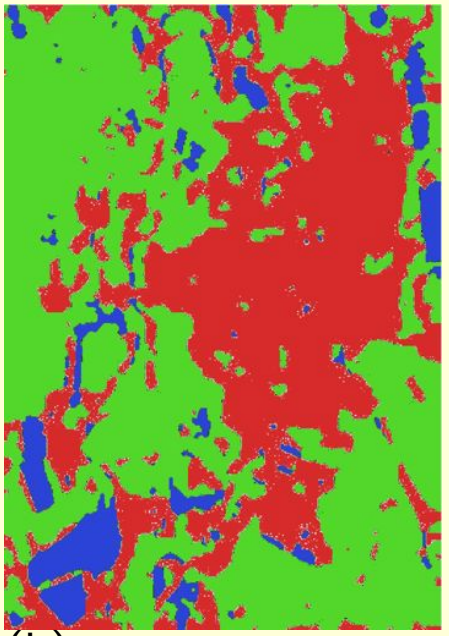

(b) MRF-based classification (©INRIA)

Example of input/output classification in 3 classes: water, urban, vegetation.

General applications in the frame of remote sensing imagery

- Land-cover or land-use maps.
- Global detection of urban areas, that are critical w.r.t. populations (risk management).
- Infrastructures mapping.
- Mapping the water before any disaster, or after a flooding.
- ...

Benchmark classifiers

- K-nearest neighbors (K-NN).
- Support Vector Machine (SVM).
- Amplitude and Texture density mixtures of MnL with CEM (ATML-CEM).
- For more information, see, e.g., J. A. Richards and X. Jia, [Remote sensing digital image analysis: an introduction], Springer-Verlag, 4^{th} edition, (2006).

K-nearest neighbors[1]

- Used to model the probability density functions.
- Integrated in a MRF model.
- Supervised estimation of the probability of a given pixel by using a majority vote on the K nearest (distance rule) known pixels.
- K estimated by cross validation.

[1] G. Shakhnarovich, P. Indyk, T. Darrell, [Nearest-neighbor methods in learning and vision: theory and practice], MIT Press, (2005).

Support Vector Machine[2]

- Well-chosen projections to reformulate the classification problem as a resolution of quadratic optimization problem, maximizing the distance between the separating border and the closest learning samples.

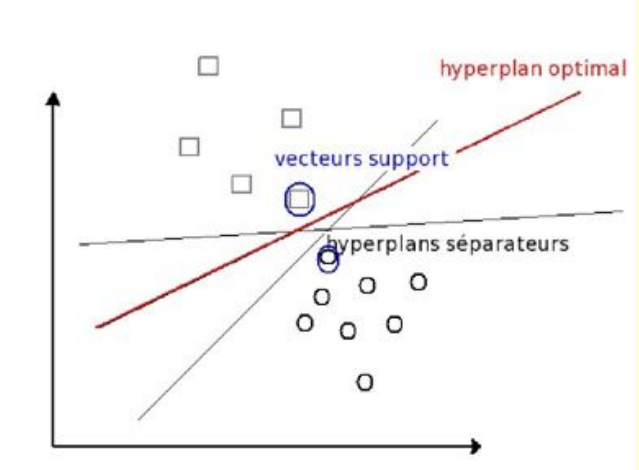

[2] V. Vapnik, [The Nature of Statistical Learning Theory], Springer, 2^{nd} edition, (2000).

ATML-CEM[3]

- Bayesian-based algorithm.
- Likelihood: Product of Experts approach to combine SAR amplitude (Nakagami density) and texture statistics (t-distribution).
- Prior probability: non-stationary Multinomial Logistic (MnL) model.
- Classification performed by using a Classification Expectation-Maximization (CEM) algorithm.

[3] K. Kayabol, A. Voisin and J. Zerubia, "SAR image classification with non-stationary multinomial logistic mixture of amplitude and texture densities,"in Proc. IEEE International Conference on Image Processing (ICIP), Brussels (Belgium) (2011). (pdf)

Contributions

2 **supervised contextual classifiers** at the same time Bayesian and Markovian:

- Shared learning: statistical modeling of the input images, by using adapted finite mixtures and d-variate copulas.
- Integration of the statistics in Markovian models: MRF with textural features[4], and hierarchical MRF integrating a prior update[5].

[4] A. Voisin, G. Moser, V. Krylov, S. B. Serpico, and J .Zerubia, "Classification of very high resolution SAR images of urban areas by dictionary-based mixture models, copulas and Markov random fields using textural features," in [Proc. of SPIE Symposium on Remote Sensing], 78300O (2010). (pdf).

[5] A. Voisin, V. Krylov, G. Moser, S. B. Serpico, and J .Zerubia, "Multichannel hierarchical image classification using multivariate copulas", in [Proc. of IS&T/SPIE Electronic Imaging], 82960K (2012). (pdf).

Overview

For each class m, and at each resolution (multi-resolution case): Build a joint PDF.

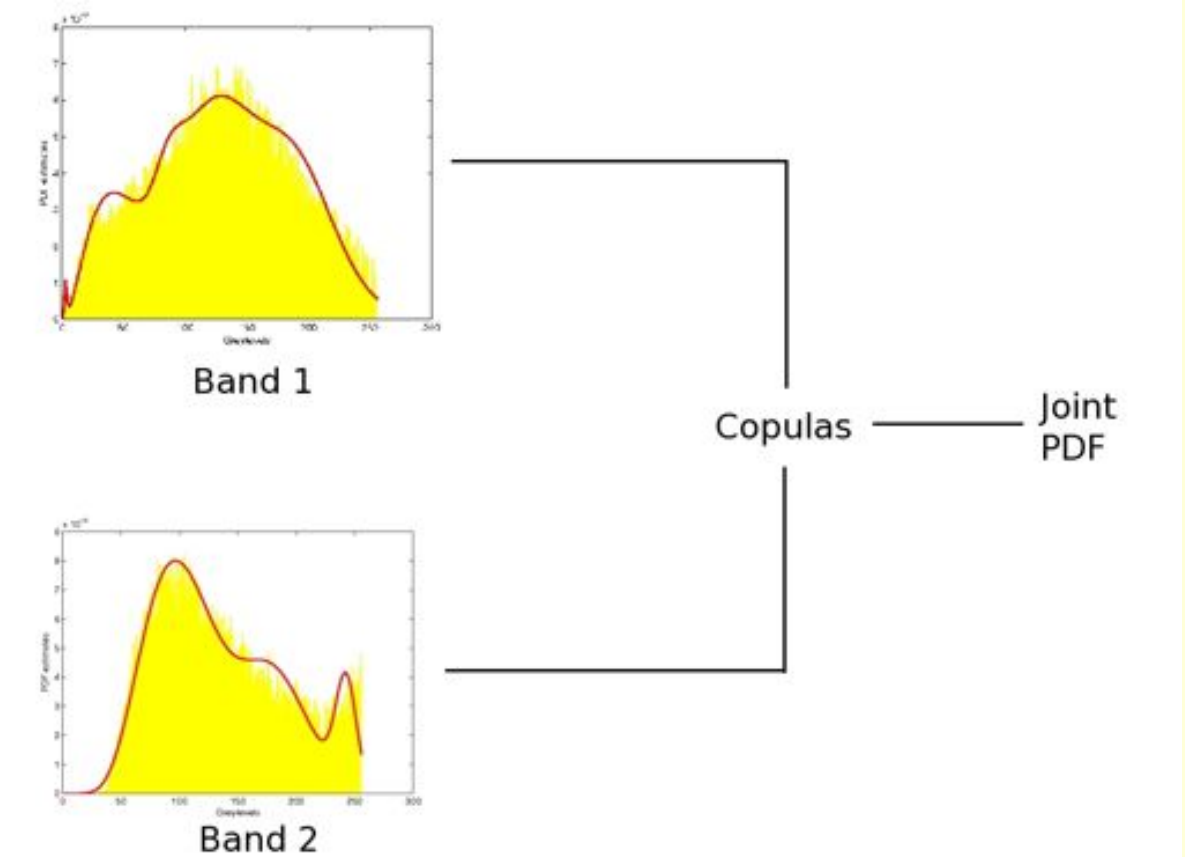

Marginal PDF modeling

For each input image, we want to estimate the distributions of each class $m \in [1; M]$. The PDF $f_m^{(j)}(z^{(j)})$ of the j^{th} input band, $j \in [1; d]$, is modeled via **finite mixtures**:

$$f_m^{(j)}(z^{(j)}) = p_m^{(j)}(z^{(j)}|\omega_m) = \sum_{i=1}^{K^{(j)}} P_{mi}^{(j)} p_{mi}^{(j)}(z^{(j)}|\theta_{mi}^{(j)}) \qquad (1)$$

$z^{(j)}$ is a greylevel, $z^{(j)} \in [0; Z-1]$

$P_{mi}^{(j)}$ are the mixing proportions such that $\sum_{i=1}^{K} P_{mi}^{(j)} = 1$

$\theta_{mi}^{(j)}$ is the set of parameters of the i^{th} PDF mixture component of the m^{th} class

Advantages of finite mixtures

- Unimodal density does not accurately model SAR amplitude statistics given their heterogeneity.
- Each component (of the sum) reflects the contribution of the different materials.

Marginal PDF modeling: Optical image case

Gaussian distribution is a usually accepted model for optical imagery:

$$p_{mi}(z|\theta_{mi}) = \frac{1}{\sqrt{2\pi\sigma_{mi}^2}} \exp\left[-\frac{(z-\mu_{mi})^2}{2\sigma_{mi}^2}\right], \quad \text{with } \theta_{mi} = \{\mu_{mi}, \sigma_{mi}^2\}. \tag{2}$$

The parameters P_{mi}, θ_{mi} are estimated within a SEM algorithm[6].

[6] G. Celeux, D. Chauveau, and J. Diebolt, "Stochastic versions of the EM algorithm: an experimental study in the mixture case," Journal of Statistical Computation and Simulation, 55(4), 287-314 (1996).

Experimental validation

(a) Original image (©GeoEye)

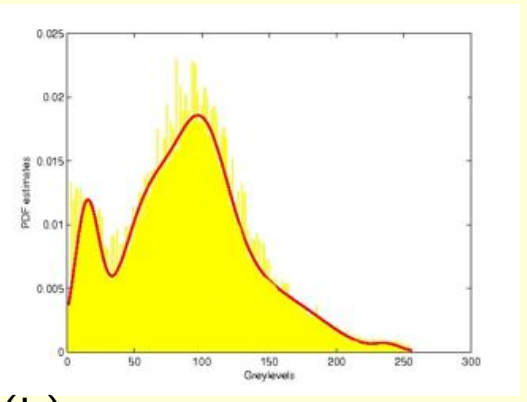

(b) Urban area modeling (©INRIA)

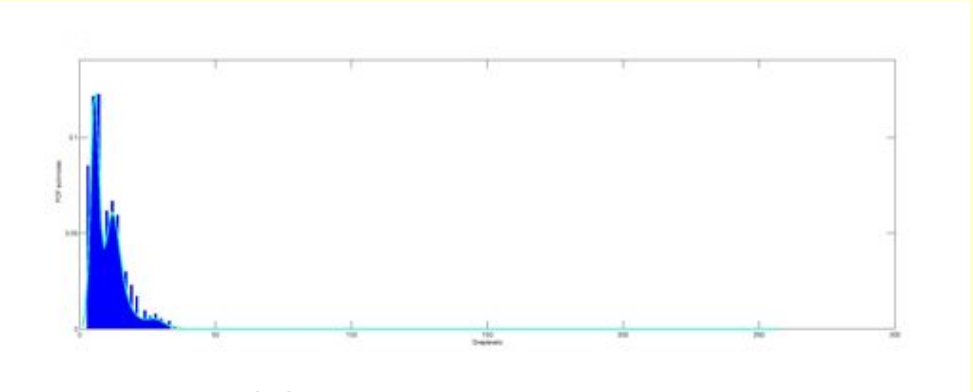

(c) Water modeling (©INRIA)

Marginal PDF modeling: SAR image case[7]

P_{mi}, θ_{mi} and K are estimated within a SEM algorithm combined to a method of log-cumulants. Best family chosen by ML.

Family	Probability density function	MoLC equations
Generalized Gamma	$p_{mi}(z\|\theta_{mi}) = \frac{\nu_{mi}}{\sigma_{mi}\Gamma(\kappa_{mi})} \left(\frac{z}{\sigma_{mi}}\right)^{\kappa_{mi}\nu_{mi}-1} \exp\left\{-\left(\frac{z}{\sigma_{mi}}\right)^{\nu_{mi}}\right\}$	$\kappa_1 = \Psi(\kappa)/\nu + \ln\sigma$ $\kappa_2 = \Psi(1,\kappa)/\nu^2$ $\kappa_3 = \Psi(2,\kappa)/\nu^3$
Log-normal	$p_{mi}(z\|\theta_{mi}) = \frac{1}{\sigma_{mi} z\sqrt{2\pi}} \exp\left[-\frac{(\ln z - m_{mi})^2}{2\sigma_{mi}^2}\right]$	$\kappa_1 = m$ $\kappa_2 = \sigma^2$
Weibull	$p_{mi}(z\|\theta_{mi}) = \frac{\eta_{mi}}{\mu_{mi}^{\eta}} z^{\eta_{mi}-1} \exp\left[-\left(\frac{z}{\mu_{mi}}\right)^{\eta_{mi}}\right]$	$\kappa_1 = \ln\mu + \Psi(1)\eta^{-1}$ $\kappa_2 = \Psi(1,1)\eta^{-2}$
Nakagami	$p_{mi}(z\|\theta_{mi}) = \frac{2}{\Gamma(L_{mi})} (\lambda_{mi} L_{mi})^{L_{mi}} z^{2L_{mi}-1} \exp\left(-\lambda_{mi} L_{mi} z^2\right)$	$2\kappa_1 = \Psi(L) - \ln\lambda L$ $4\kappa_2 = \Psi(1,L)$

[7] Krylov, V., Moser, G., Serpico, S. B., and Zerubia, J., "Supervised high resolution dual polarization SAR image classification by finite mixtures and copulas," IEEE J-STSP, 5(3), 554-566 (2011).

Marginal PDF modeling: SAR image case

Method of log-cumulants[8]:

- Estimation of the moments given a training set, and equation system solving.
- Applicability for the generalized gamma distribution[9]: $\kappa_{2mi}^t \geqslant 0.63(\kappa_{3mi}^t)^{(2/3)}$.

K estimation: For each i, if $P_{mi}^{t+1} <$ threshold then K^{t+1} is decremented.

[8] C. Tison, J.-M. Nicolas, F. Tupin and H. Maitre, "A new statistical model for Markovian classification of urban areas in high-resolution SAR images," IEEE Trans. Geosci. Remote Sens. 42(10), 2046-2057 (2004).

[9] V. Krylov, G. Moser, S. B. Serpico and J. Zerubia, "On the method of logarithmic cumulants for parametric probability density function estimation," Research report 7666, INRIA, France (2011).

Modified SEM algorithm - Settings

- Initialization: $K_{max} = 6$.
- Stop criterion: Maximum number of iterations reached (SEM: convergence in law to a stationary distribution).

Experimental validation

(a) Amiens (©ASI, 2011)

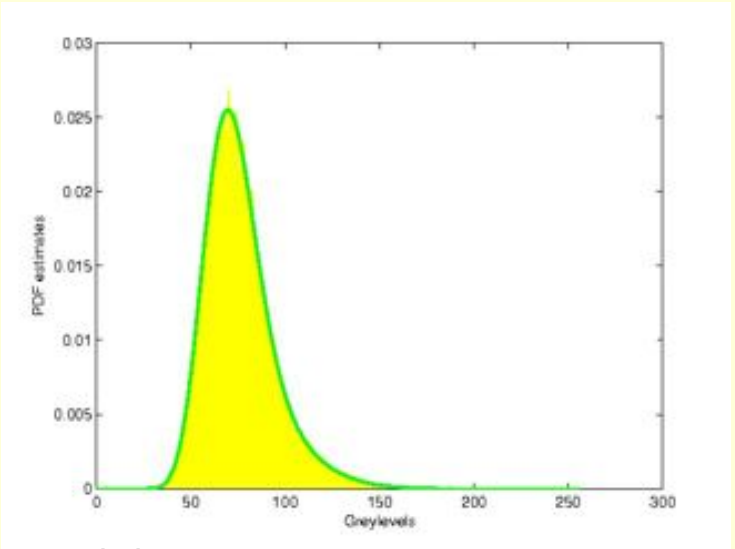

(b) Vegetation modeling (©INRIA)

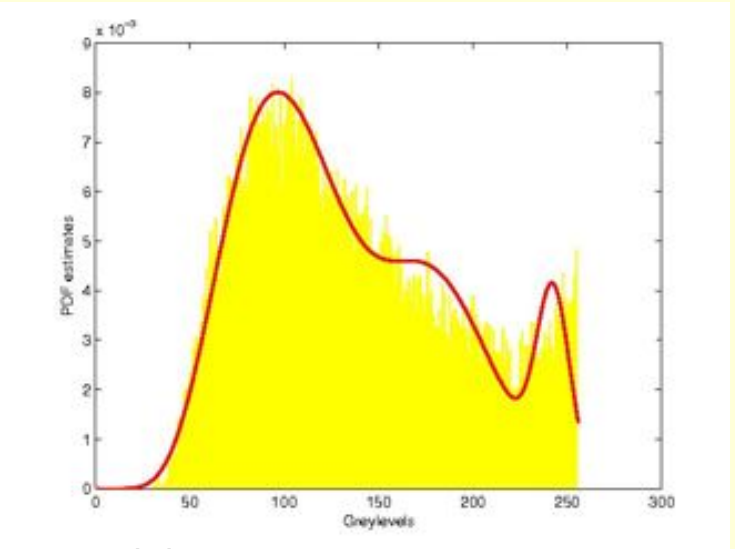

(c) Urban modeling (©INRIA)

Joint PDF modeling by resorting to multivariate copulas

Usefulness: Find a **joint class-conditional model** to statistically group the input images (at a given resolution).
According to Sklar's theorem[10]:

$$p_m(z^{(1)},...,z^{(d)}|\omega_m) = \prod_{j=1}^{d} p_m^{(j)}(z^{(j)}|\omega_m) \times \frac{\partial^d C}{\partial z^{(1)}...\partial z^{(d)}}(F^{(1)}(z^{(1)}|\omega_m),...,F^{(d)}(z^{(d)}|\omega_m)), \quad (3)$$

d corresponds to the total number of inputs.

[10] Nelsen, R. B., [An introduction to copulas], Springer, New York, 2nd ed. (2006).

Multivariate copulas dictionary

Copula dictionary, $\theta(\tau)$ and τ intervals.

Copula	$C(u_1, ..., u_d)$	$\theta(\tau)$	τ interval
Clayton	$\left[\left(\sum_{i=1}^{d} u_i^{-\theta}\right) - d + 1\right]^{-1/\theta}$	$\theta = \frac{2\tau}{1-\tau}$	$\tau \in]0; 1]$
AMH	$\frac{\prod_{i=1}^{d} u_i}{1-\theta\prod_{i=1}^{d}(1-u_i)}$	$\tau = \frac{3\theta-2}{3\theta} - \frac{2}{3}\left(1-\frac{1}{\theta}\right)^2 \ln(1-\theta)$	$\tau \in [-0,182; \frac{1}{3}]$
Gumbel	$\exp\left(-\left[\sum_{i=1}^{d}(-\ln u_i)^{\theta}\right]^{1/\theta}\right)$	$\theta = \frac{1}{1-\tau}$	$\tau \in [0; 1]$

Clayton copula density example

$$c(u_1, ..., u_d) = \prod_{j=1}^{d} u_j^{-(\alpha+1)} \cdot \prod_{n=0}^{d-1} (1 + \alpha n) \cdot (\sum_{j=1}^{d} u_j^{-\alpha} - d + 1)^{(\frac{-1-d\alpha}{\alpha})}. \quad (4)$$

Copula choice

- Kendall's τ empirical estimation.
- Estimation of the **copula parameters** given the equations.
- For each class: statistical test applied to the observations of the different input bands (χ-square test[11]) to find the **best-fitting copula family**.

[11] E. Lehmann and J. Romano, [Testing statistical hypothesis], Springer, 3rd ed. (2007).

General presentation

- Classification of multi-band, single-resolution acquisitions into M classes.
- Contextual information via MRF.
- Use the Bayesian formulation:

$$p_m(x = \omega_m|y) \propto p(x) \times p_m(y|x = \omega_m)$$

Prior probabilities

For each class $m \in [1, M]$ (Gibbs):

$$p(x_s) = \frac{\exp(-U(x_s = \omega_m))}{\sum_{j=1}^{M} \exp(-U(x_s = \omega_j))} \tag{5}$$

Potts model:

$$U(x_s, \beta) = \sum_{s' \in S} \left[-\beta \sum_{s:\{s,s'\} \in C} \delta_{x_s = x'_s} \right] \tag{6}$$

where

$$\beta > 0 \quad \text{and} \quad \delta_{x_s = x_{s'}} = \begin{cases} 1, & \text{if } x_s = x_{s'} \\ 0, & \text{otherwise} \end{cases}$$

s and s' belong to the same clique C.

Optimization

- Need to maximize the posterior probability to find the labels.
- Here: **minimization of the energy function**:

$$H(x = \omega_m | y, \beta) = \sum_{t \in S} \left[-\log p_m(y_t | x_t = \omega_m) - \beta \sum_{s:\{s,t\} \in C} \delta_{x_s = x_t} \right] \quad (7)$$

Tools:

- Modified Metropolis dynamics[12].
- Graph-cuts.

[12] Berthod, M., Kato, Z., Yu, S., and Zerubia, J., "Bayesian image classification using Markov random fields," Image and Vision Computing 14(4), 285-295 (1996).

Textural features[13]

- Problem: single-pol SAR images.
- Aim: Improve the classification accuracy by integrating some additional information: **textural features**.

[13] Voisin, A., Moser, G., Krylov, V., Serpico, S. B., and Zerubia, J., "Classification of very high resolution SAR images of urban areas by dictionary-based mixture models, copulas and Markov random fields using textural features," in [Proc. of SPIE Symposium on Remote Sensing], 78300O (2010).

Textural features

- Well-adapted textural feature: Haralick's GLCM variance[14].
- Urban area discrimination.
- Principle: Moving $w \times w$ window, and estimation of the value of the central pixel by using its neighborhood (calculation of second-order statistics).
- Same statistical model as for SAR imagery (no models available).

[14] R. M. Haralick, K. Shanmugam and I. Dinstein, "Textural features for image classification," IEEE TRans. Syst., Man, Cybern. 3(6), 610-621 (1973).

Experimental settings

- Number of classes M fixed by the user.
- MRF β parameter manually fixed ($\beta = 1.3$).
- Windows of size $w = 5$ for textural feature extraction.
- Ground truth sets represent 5% of the whole image.

Single-pol Cavallermaggiore

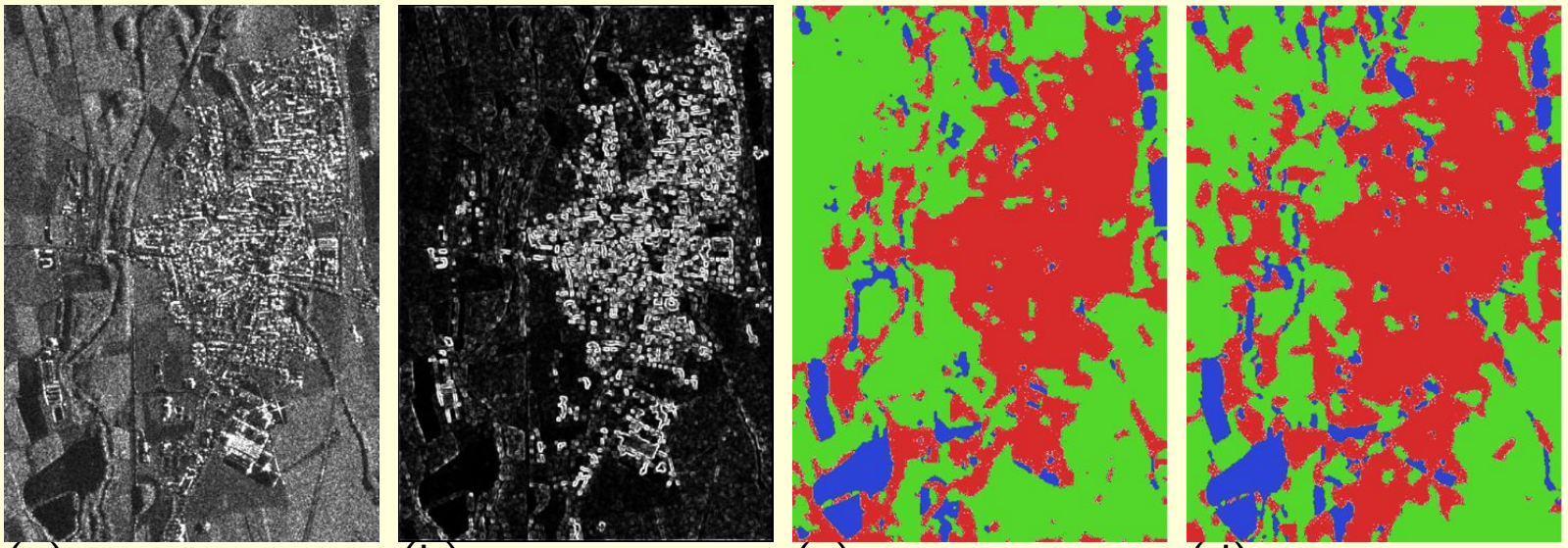

(a) Original SAR image (COSMO-SkyMed, ©ASI)

(b) Extracted GLCM variance textural feature

(c) Proposed method (with textural features) (©INRIA)

(d) Proposed method (without textural features) (©INRIA)

Classification results, 3 classes: water, urban, vegetation.

Single-pol Cavallermaggiore

Accuracy for each of the 3 classes and overall results:

	Water	Urban	Vegetation	**Overall**
Proposed method with texture	98.62%	98.42%	100%	**99.01%**
Proposed method, no texture	95.96%	98.88%	84.65%	**93.16%**

Single-pol Rosenheim

(a) SAR image (TerraSAR-X, ©Infoterra)

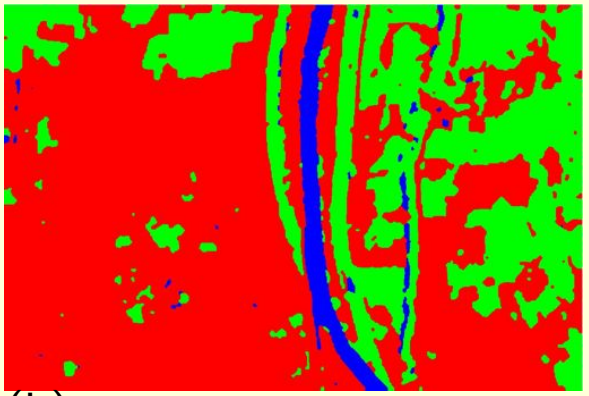

(b) Proposed MRF method (©INRIA)

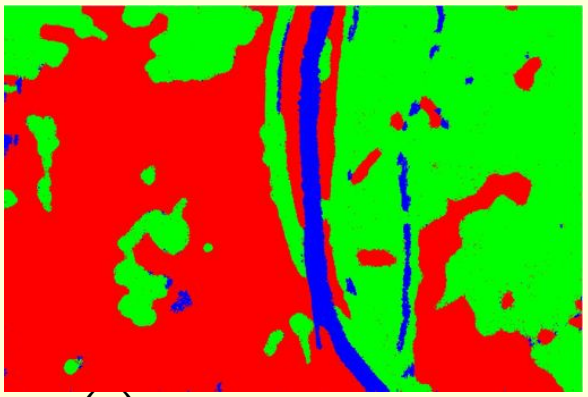

(c) ATML-CEM (©INRIA)

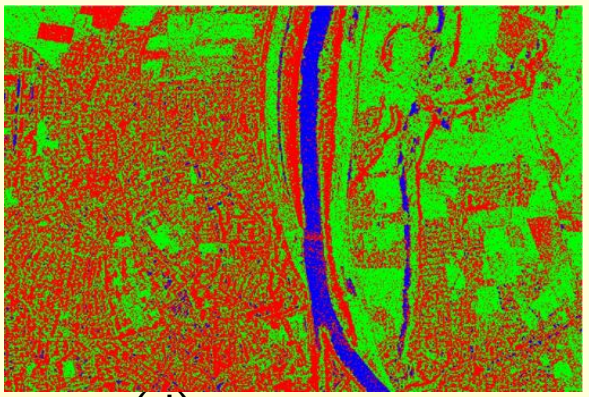

(d) SVM (©INRIA)

Single-pol Rosenheim

Accuracy for each of the 3 classes and overall results:

	Water	Urban	Vegetation	**Overall**
Proposed method, with texture	91.28%	98.82%	93.53%	**94.54%**
Proposed method, no texture	92.95%	98.32%	81.33%	**90.87%**
K-NN-MRF, with texture	90.56%	98.49%	94.99%	**94.68%**

General presentation: Example of multisensor data classification

(a) SAR image (©ASI, 2010) (2.5 m)

(b) Optical image (©GeoEye, 2010) (65 cm)

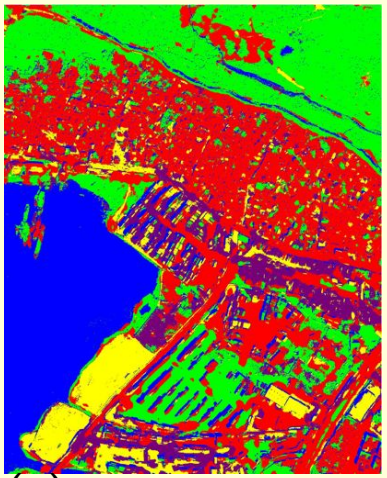

(c) Hierarchical MRF-based classification (optical + SAR) (©INRIA)

Example of classification result for a multi-sensor acquisition over the Port-au-Prince quay (Haiti).

General presentation: Considered data

- Classification of coregistered mono-/multi-band, multi-resolution and/or multi-sensor (SAR, optical) acquisitions into M classes
- **Hierarchical graph**: use multi-resolution data.
- **Flexible** enough to take into account different kinds of statistics (multi-sensor effects).

General presentation: Hierarchical method

- Classification: Estimate the labels X at the finest resolution (here, level 0) given all the observations.
- Quad-tree structure: causality that allows to use a non-iterative algorithm.
- MPM (marginal posterior mode)[15] instead of MAP to avoid underflow problems.
- MPM penalizes the errors according to their number and the scale at which they occur.

[15] Laferte, J.-M., Perez, P., and Heitz, F., "Discrete Markov modeling and inference on the quad-tree," IEEE Trans. Image Process. 9(3), 390-404 (2000).

Notations

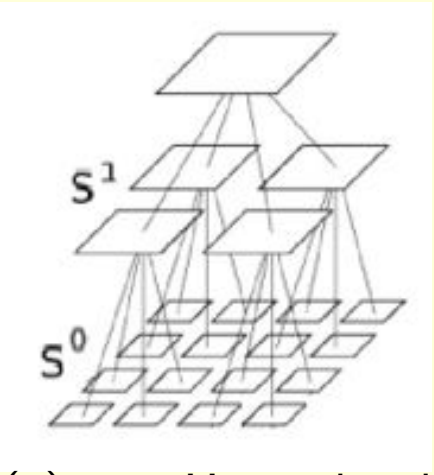

(a) Hierarchical model structure: quad-tree.

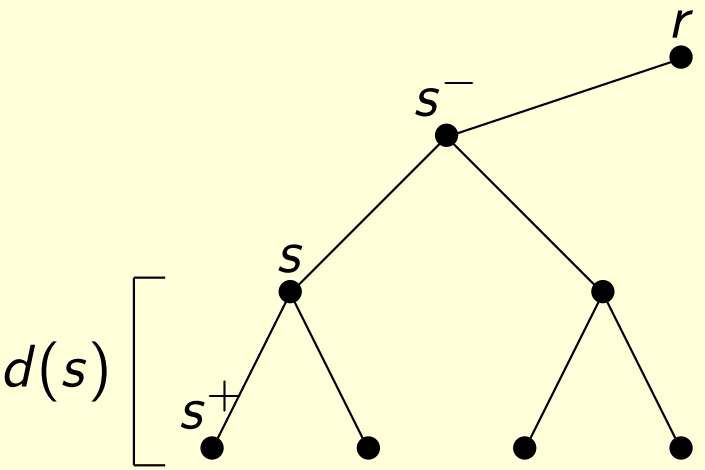

(b) Quad-tree notations.

Notations

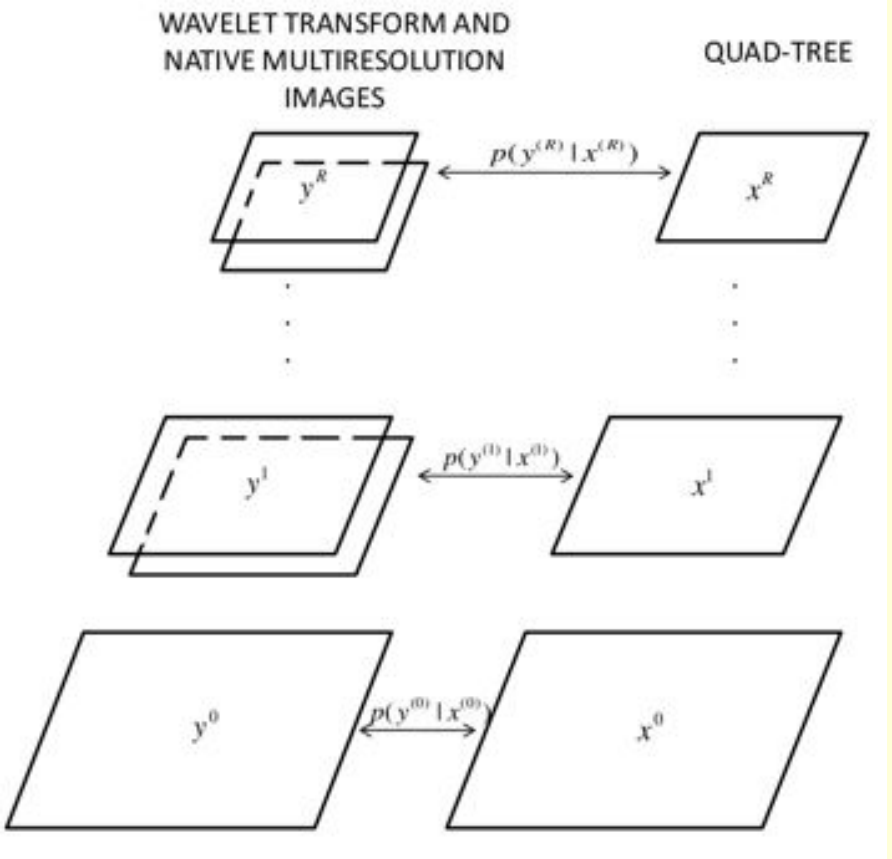

Generic hierarchical graph-based model of the quad-tree.

Initial MPM scheme

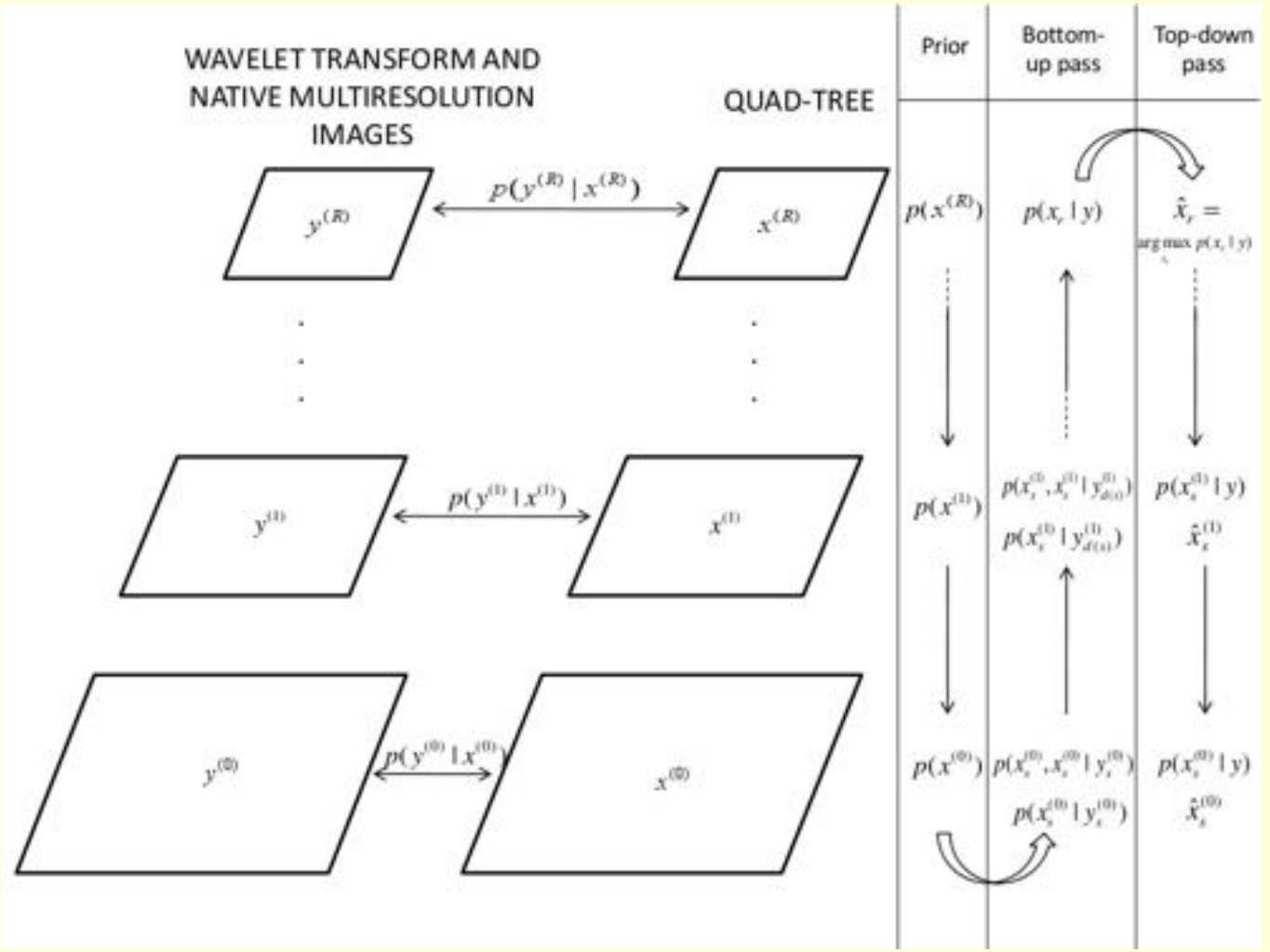

Global scheme - prior update[17]

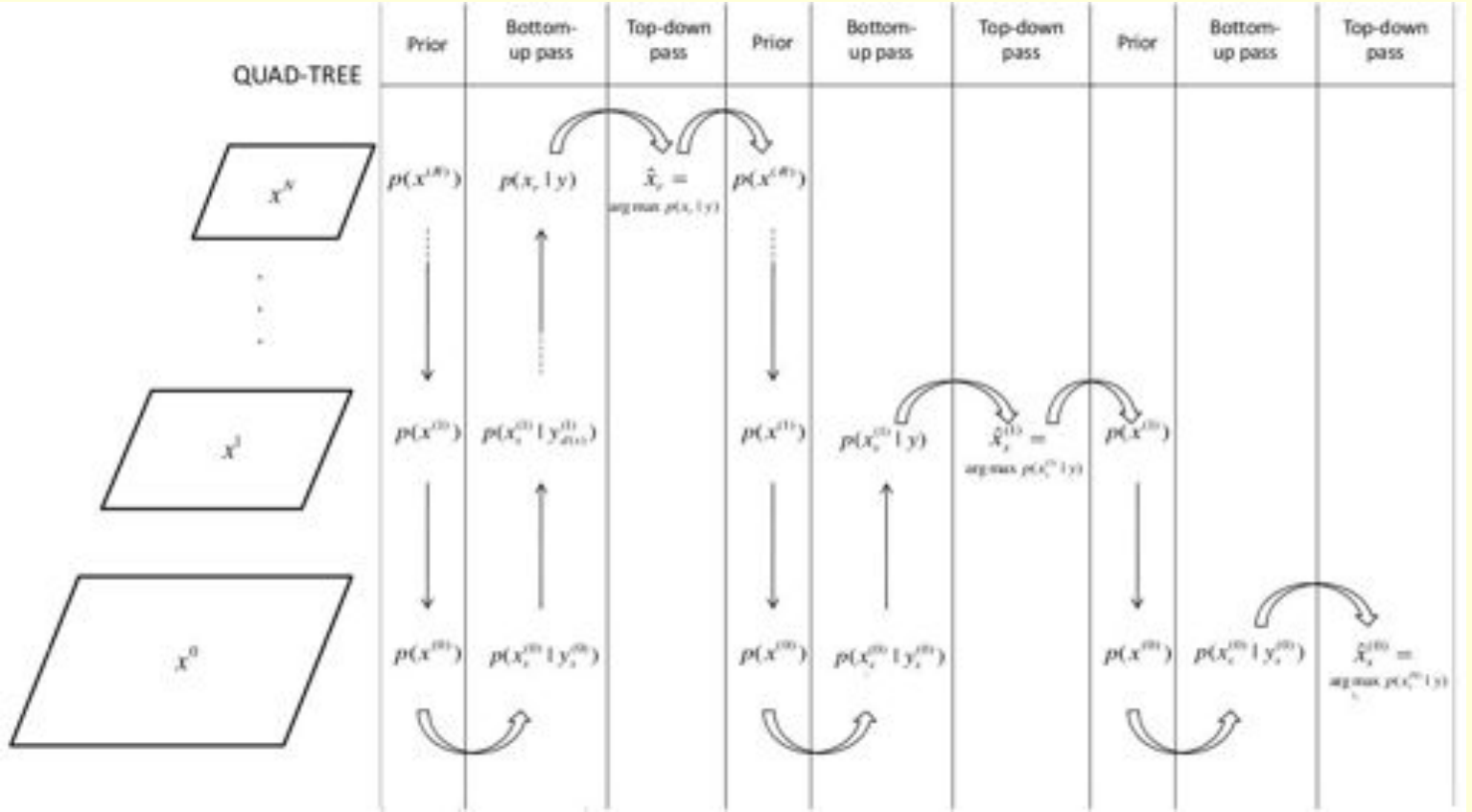

[17] A. Voisin, V. Krylov, G. Moser, S.B. Serpico and J. Zerubia, "Classification of Very High Resolution SAR Images of Urban Areas Using Copulas and Texture in a Hierarchical Markov Random Field Model," IEEE Geoscience and Remote Sensing Letters, 10(1), 96-100 (2013). (pdf).

Optimization

- Need to maximize the posterior probability at the coarsest scale (top-down pass).
- Tool: modified Metropolis dynamics.

Posterior probability

Expression of the partial posterior probability (bottom-up pass):

$$p(x_s|y_{d(s)}) = \frac{1}{Z} p(y_s|x_s)p(x_s) \prod_{t \in s^+} \sum_{x_t} \left[\frac{p(x_t|y_{d(t)})}{p(x_t)} p(x_t|x_s) \right]. \quad (8)$$

Thus, we need to define the prior probabilities, the transition probabilities. The likelihood has already been defined (joint PDF at each level of the tree).

Transition probabilities

For all sites $s \in S$ and all scales $n \in [0; R-1]$, R corresponding to the root[18],

$$p(x_s = \omega_m | x_{s^-} = \omega_k) = \begin{cases} \theta_n, & \text{if } \omega_m = \omega_k \\ \frac{1-\theta_n}{M-1}, & \text{otherwise} \end{cases} . \quad (9)$$

The transition probabilities determine the hierarchical MRF since they represent the causality of the statistical interactions between the different levels of the tree.

[18] Bouman, C. and Shapiro, M., "A multiscale random field model for Bayesian image segmentation," IEEE Trans. Image Process. 3(2), 162-177 (1994).

Prior probabilities

Prior probabilities at the coarsest level: Updated. Prior probability

at level n in $[0; R-1]$:

$$p(x_s^n) = \sum_{x_{s^-}^n} p(x_s^n | x_{s^-}^n) p(x_{s^-}^n). \tag{10}$$

Experimental settings

- Number of classes M fixed by the user.
- $\theta_n = 0.85$ (transition probability).
- For native single-resolution images, the multi-resolution acquisitions are obtained by WT (Db10[19] and Haar) on $R = 2$ levels.

[19] I. Daubechies, "Orthonormal bases of compactly supported wavelets," Communications on Pure and Applied Mathematics, 41(7), 909-996 (1988).

Single-pol mono-resolution Cavallermaggiore

(a) SAR image (©ASI)

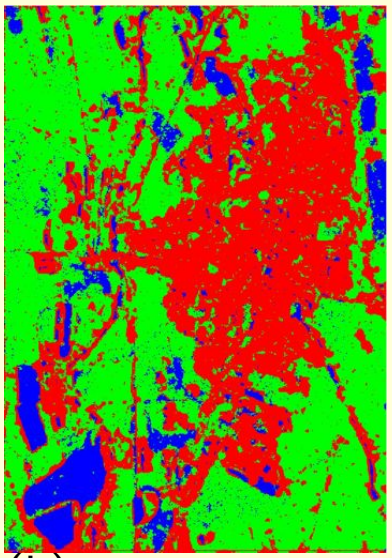

(b) Hierarchical MRF with textural feature (©INRIA)

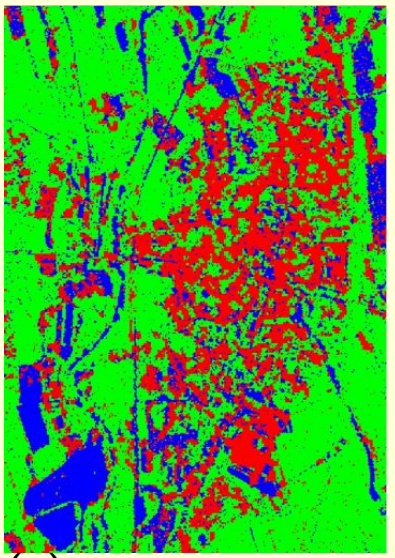

(c) Initial MPM method (©INRIA)

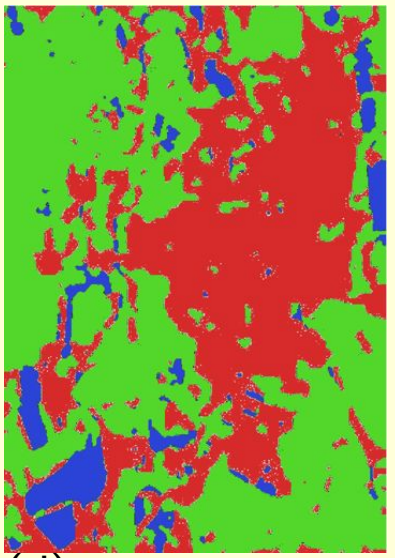

(d) MRF-based classif. (©INRIA)

Classification results, 3 classes: water, urban, vegetation.

Single-pol mono-resolution Cavallermaggiore

Accuracy for each of the 3 classes and overall results:

	Water	Urban	Vegetation	**Overall**
Hierarchical MRF	98.20%	91.80%	98.35%	**96.12%**
Hierarchical MRF, no texture	98.37%	70.05%	97.99%	**88.80%**
Initial MPM method	94.84%	63.24%	94.60%	**84.23%**
MRF-based classif.	98.62%	98.42%	100%	**99.01%**

Histological RGB image of the skin

Considered image:

- RGB histological image of the skin provided by Galderma.
- 550×1020 pixels.

Histological RGB image of the skin

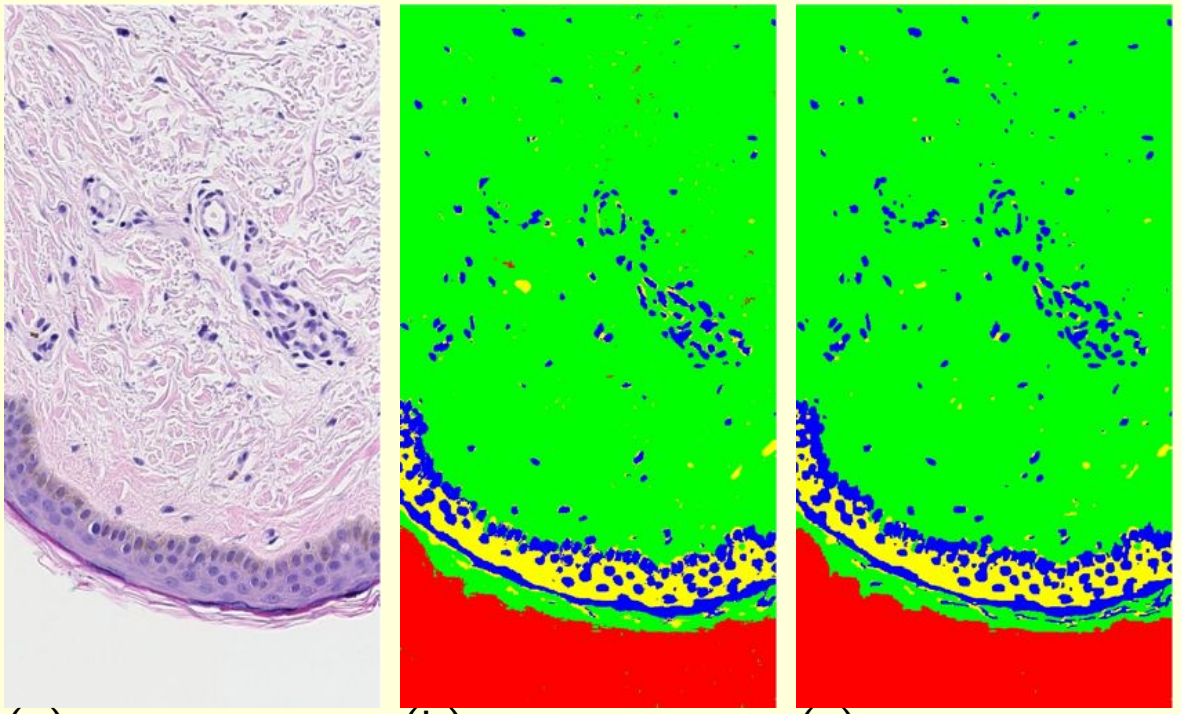

(a) Original RGB image (©Galderma) (b) Hierarchical MRF classif. (©INRIA) (c) MRF-based classif. (©INRIA)

Histological image and classification results, 4 classes: cytoplasm, nuclei, background, dermis matrix, collagen and stratum corneum keratin.

Histological RGB image of the skin

Accuracy for each of the 4 classes and overall results:

	Nuclei	Dermis	Background	Cytoplasm	**Overall**
Hierarchical MRF	97.08%	99.87%	97.71%	97.13%	**97.95%**
Single-scale MRF	99.92%	99.97%	97.72%	96.65%	**98.56%**

- Softwares deposited to APP and transferred to Galderma and IPAL Singapore.
- Results in the book: Z. Kato and J. Zerubia, [Markov random fields in image segmentation], Now Publishers, World Scientific (2012).

Multi-resolution SAR acquisition of Amiens (France)

Considered image:

- 2 single-pol COSMO-SkyMed SAR images of the city of Amiens (France) (©ASI, 2011):
  - a StripMap acquisition (2.5 m pixel spacing), HH polarized, geocoded, single-look image. 510×1200 pixels.
  - a PingPong acquisition (5 m pixel spacing), HH polarized, geocoded, 255×600 pixels.
- $R = 1$.
- at each scale, a GLCM textural feature is extracted and is added as a second channel.

Multi-resolution SAR acquisition of Amiens (France)

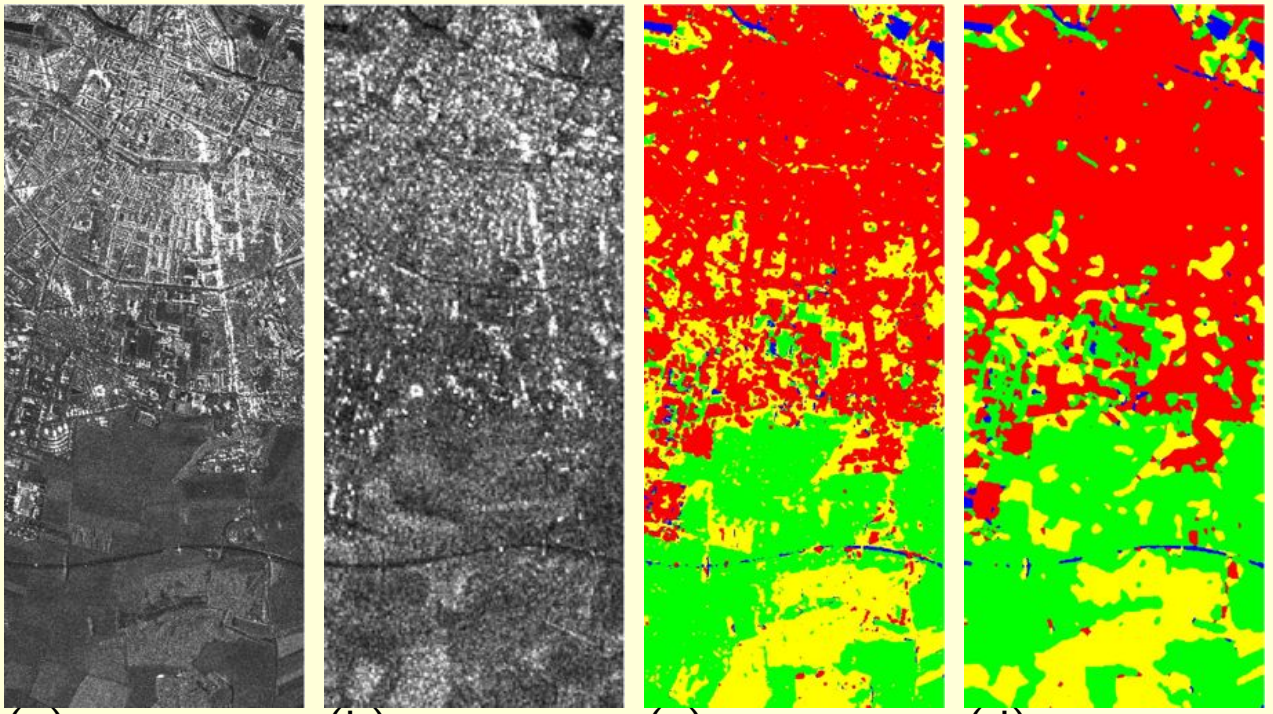

(a) StripMap SAR image (©ASI, 2011) (b) PingPong SAR image (©ASI, 2011) (c) Hierarchical MRF-based classifier (©INRIA) (d) MRF-based classifier (©INRIA)

Classification results, 4 classes: water, urban, vegetation and trees.

Multi-sensor acquisition of Port-au-Prince (Haiti)

2 coregistered images of the quay of Port-au-Prince (Haiti):

- a single-polarized COSMO-SkyMed SAR image (©ASI, 2010), HH polarization, StripMap acquisition mode (2.5 m pixel spacing), geocoded, single-look of 320×400 pixels.
- a pan-sharpened (1-band) GeoEye acquisition (©GeoEye, 2010, 0.65 m pixel spacing) of 1280×1600 pixels.

Multi-sensor acquisition of Port-au-Prince (Haiti)

(a) Optical image (©GeoEye, 2010)

(b) Hierarchical MRF-based classifier (©INRIA)

(c) SVM (©INRIA)

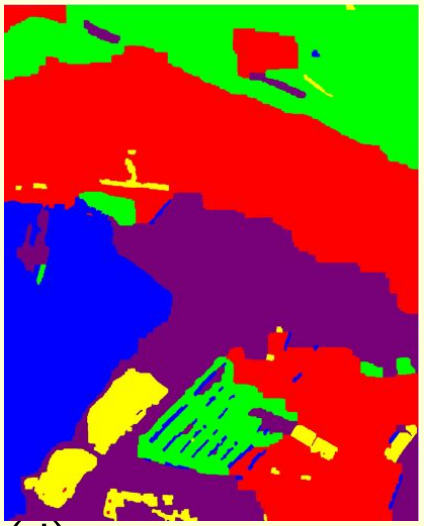

(d) MRF-based classifier (©INRIA)

Classification results, 5 classes: water, urban, vegetation, sand, and containers.

Multi-sensor acquisition of Port-au-Prince (Haiti)

Accuracy for each of the 4 classes and overall results:

	Water	Urban	Veget.	Sand	Contain.	**Overall**
Hierarchical MRF	100%	75.24%	87.16%	98.89%	49.31%	**82.12%**
Hierarchical MRF (Pan. only)	100%	67.12%	86.89%	98.83%	41.90%	**78.95%**
MRF-based classif.	100%	100%	81.42%	99.94%	59.62%	**88.20%**

Conclusion

- Classification of multi-band, multi-resolution, and/or multi-sensor acquisitions.
- Well-adapted joint PDF modeling.
- Satisfying classification results obtained by using these Markovian methods. Smoothing effects of the MRF. Details provided by the hierarchical MRF.
- Selection of the best method according to the user.

Perspectives (methodological)

- *Perspective* 1*:* Graphical validation of the copulas by using Kendall-plots[20].

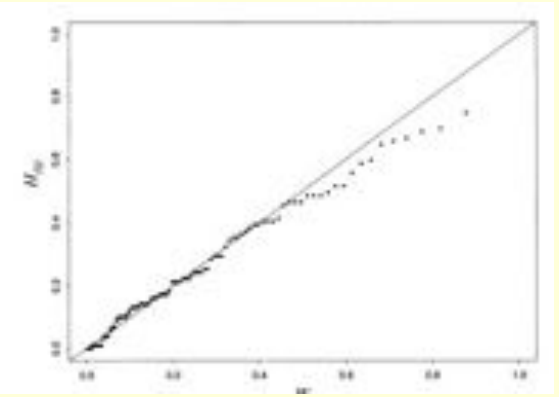

K-plot in the case of independent data.

[20] C. Genest, J.-C. Boies, "Detecting dependence with Kendall plots," The American Statistician, 57(4), 275-284 (2003).

Perspectives (methodological)

- *Perspective* 2*:* Extension of the copula dictionary.
- *Perspective* 3*:* Adaptive neighborhood for prior probabilities[21] to take into account the local geometry.
- *Perspective* 4*:* Use another type of quad-tree to overcome the required dyadic decomposition. Relax the causality constraint?

[21] P. Zhong, F. Lui, and R. Wang, "A new MRF framework with dual adaptive contexts for image segmentation," in International Conference on Computational Intelligence and Security, pp 351-355 (2007).

Perspectives (computational)

- *Perspective* 5*:* Decrease of the computational time by using some graphical methods, exploiting the graph structure.

Acknowledgments

We would like to thank:

- Prof. Serpico and Dr. Moser for the fruitful collaboration.
- The Direction Générale de l'Armement (DGA, France) and Institut National de Recherche en Informatique et Automatique (INRIA, France) for the financial support.
- The Italian Space Agency (ASI) for providing the COSMO-SkyMed images.
- The German space agency (DLR) for providing the TerraSAR-X images.
- GeoEye Inc. and Google crisis response for providing the GeoEye images.
- Galderma R&D Early Development (Sophia Antipolis, France) for providing the histological images.